Stem Cell Reports, Volume *5*

Supplemental Information

Progressive Chromatin Condensation and H3K9 Methylation Regulate the Differentiation of Embryonic and Hematopoietic Stem Cells

Fernando Ugarte, Rebekah Sousae, Bertrand Cinquin, Eric W. Martin, Jana Krietsch, Gabriela Sanchez, Margaux Inman, Herman Tsang, Matthew Warr, Emmanuelle Passegué, Carolyn A. Larabell, and E. Camilla Forsberg

Table S1 – Differential expression of genes involved in cell migration and chemotaxis, related to Figure 5

Gene symbol	log2 Fold Change	p-value
Elane	1.89	4.14E-18
Ndn	-1.66	4.91E-10
Itgam	1.51	7.44E-10
Adora3	2.63	7.46E-09
Itga3	-2.00	8.42E-09
Ccr1	1.98	1.82E-07
Thbs1	-1.42	8.21E-07
Myh10	-1.04	2.33E-06
Nkx2-3	-1.14	4.86E-06
Apbb1	-1.57	6.10E-06
Ecscr	-1.51	8.93E-06
Selp	1.00	3.83E-05
Syne2	-0.93	4.30E-05
Ccl9	0.83	5.91E-05
C3ar1	1.46	1.24E-04
Prkg1	-0.89	1.45E-04
Cd2ap	-0.81	5.91E-04
S100a9	-1.71	7.52E-04
Lsp1	0.74	7.89E-04
Cxcr2	0.98	9.46E-04
S100a8	-1.62	9.85E-04
Robo1	-1.02	1.11E-03
Cx3cr1	1.17	1.54E-03
Fcer1g	0.68	2.05E-03
Fcgr3	0.79	2.14E-03
Plau	-0.99	2.22E-03
Nrp1	0.71	2.82E-03
Zeb2	0.65	3.97E-03

Table S2 - ChIP-qPCR primer sequences, related to Figure 5

Gene symbol	**Forward primer 5'→ 3'**	**Reverse primer 5'→ 3'**
Gata1	TGGACACTGGACTCCACAGA	CGCCCTTCCTGTCTATCCTG
Sox6	TCAGTTGACCAGAGTGCAGC	CCTAGGACTCTCTCCTGCGT
Fgf3	CTTCGGTTCTGTTGCCCTCT	AAAGGTGGGTGAGGCAGATG
Itga2b	AGAGCTGTACAACTGTGGGC	TGAAAGTCCAGCCACCATCC
Flt3	GCTGGAGAGGTAGCTGTGTG	CTGCACACCACAGTGAGACT
Ndn	GGATGTGCTCCCAACATGGA	ACCTTTTTGCCCTGCTCACT
EGR1	AGAACCAACAGATCCTGGCG	AAGGCTATTCCCTCCGTCCT
Myh10	AGCCCTAGGGGCTATGACAA	GCAGAGAAGACCAGAGAGCG

Supplemental Figure 1

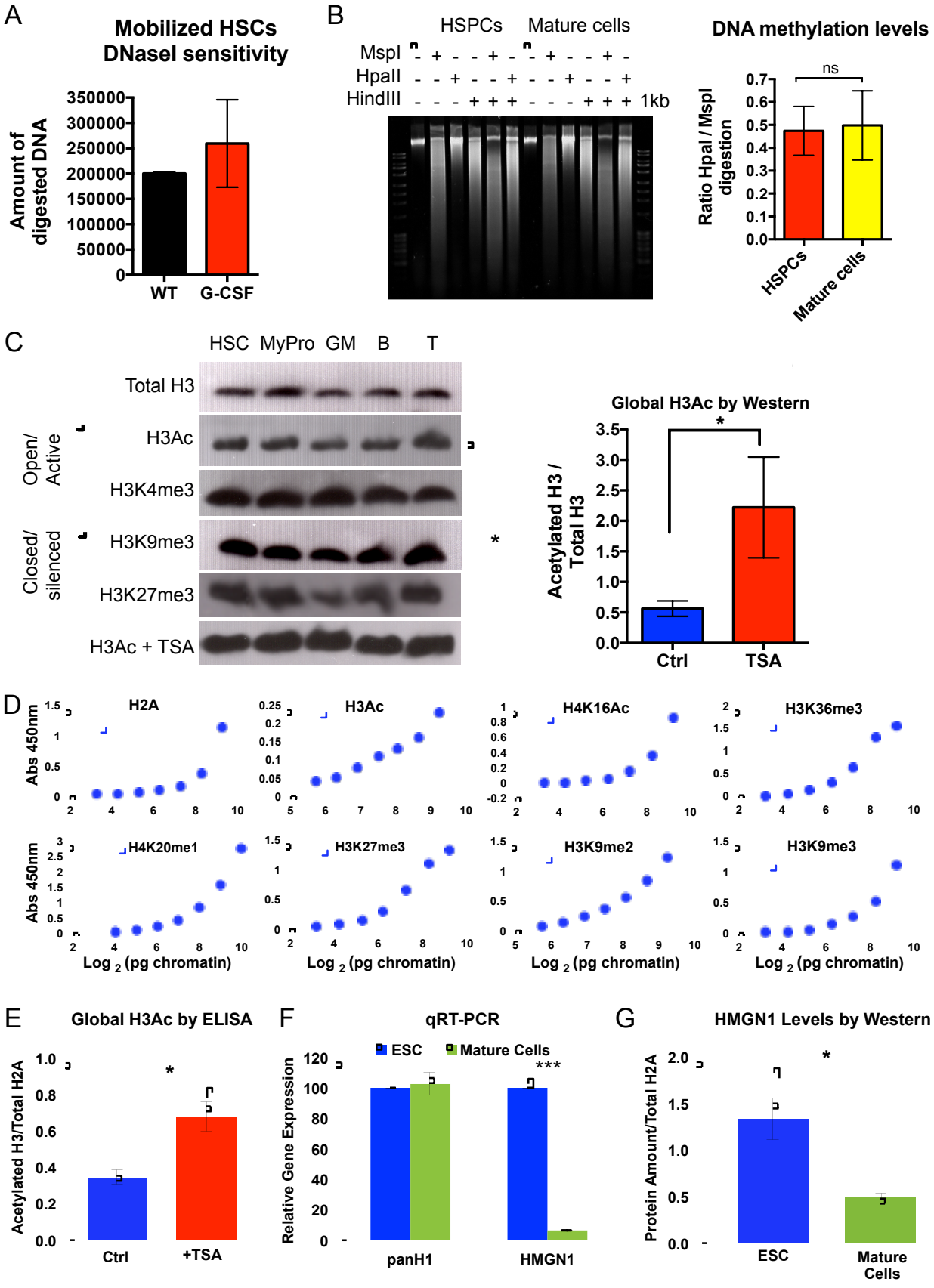

Supplemental Figure 1. Lack of changes in global chromatin parameters with cell cycling or differentiation; related to Figure 1

(A) DNaseI sensitivity does not increase significantly in HSCs (KLS FLK2$^-$ BM cells) induced to proliferate *in vivo*, indicating that cell cycle status does not strongly influence DNaseI sensitivity. HSCs were obtained from the BM of untreated control mice or from mice treated with cytoxan and G-CSF, as described previously (Morrison et al., 1997; Smith-Berdan et al., 2011). HSCs were then treated with DNaseI, as in Figure 1A. n = 2 independent experiments.

(B) DNA methylation levels are not significantly different between HSPCs and mature cells, quantified as the relative amount of DNA digestion by the methylation-sensitive enzyme HpaII relative to its methylation-insensitive isoschizomer MspI. DNA digestion was quantified as in Figure 1A and B. n = 3 independent experiments.

(C) The global abundance of histone marks is not different between HSCs, myeloid progenitors (MyPro, defined as ckit$^+$Lineage$^-$SCA1$^-$ BM cells), GM, B and T cells. Acetylation of histone H3 increased significantly with a 1-hour treatment of cells with the histone deacetylase inhibitor Trichostatin A (TSA), as expected. n = 3 independent experiments.

(D) Ability of histone antibodies to detect increasing amounts of nucleosomes in ELISA. Representative dose-titration assays for each histone modification show that the absorbance signal at 450 nm increases with increasing amount of chromatin loaded in each well.

(E) Detection of histone H3 acetylation changes by ELISA. After a 1-hour treatment of ESCs with TSA, histone H3 acetylation significantly increased as assayed by NU-ELISA. n = 3 independent experiments.

(F) Expression of histone *H1* and *Hmgn1* by qRT-PCR in ESCs and mature bone marrow cells. Histone *H1* mRNA levels were equivalent between ESCs and lineage-positive bone marrow cells, whereas *Hmgn1* mRNA was significantly higher in ESCs. n = 3 independent experiments, each performed in triplicate.

(G) HMGN1 protein abundance is higher in ESCs compared to mature bone marrow cells. Protein levels were assessed by semi-quantitative immunoblotting of whole cell extracts from ESCs or lineage-positive bone marrow cells. n = 3 independent experiments.

Error bars represent standard error of the mean (SEM). *$p < 0.05$. ns, not significant.

Supplemental Figure 2

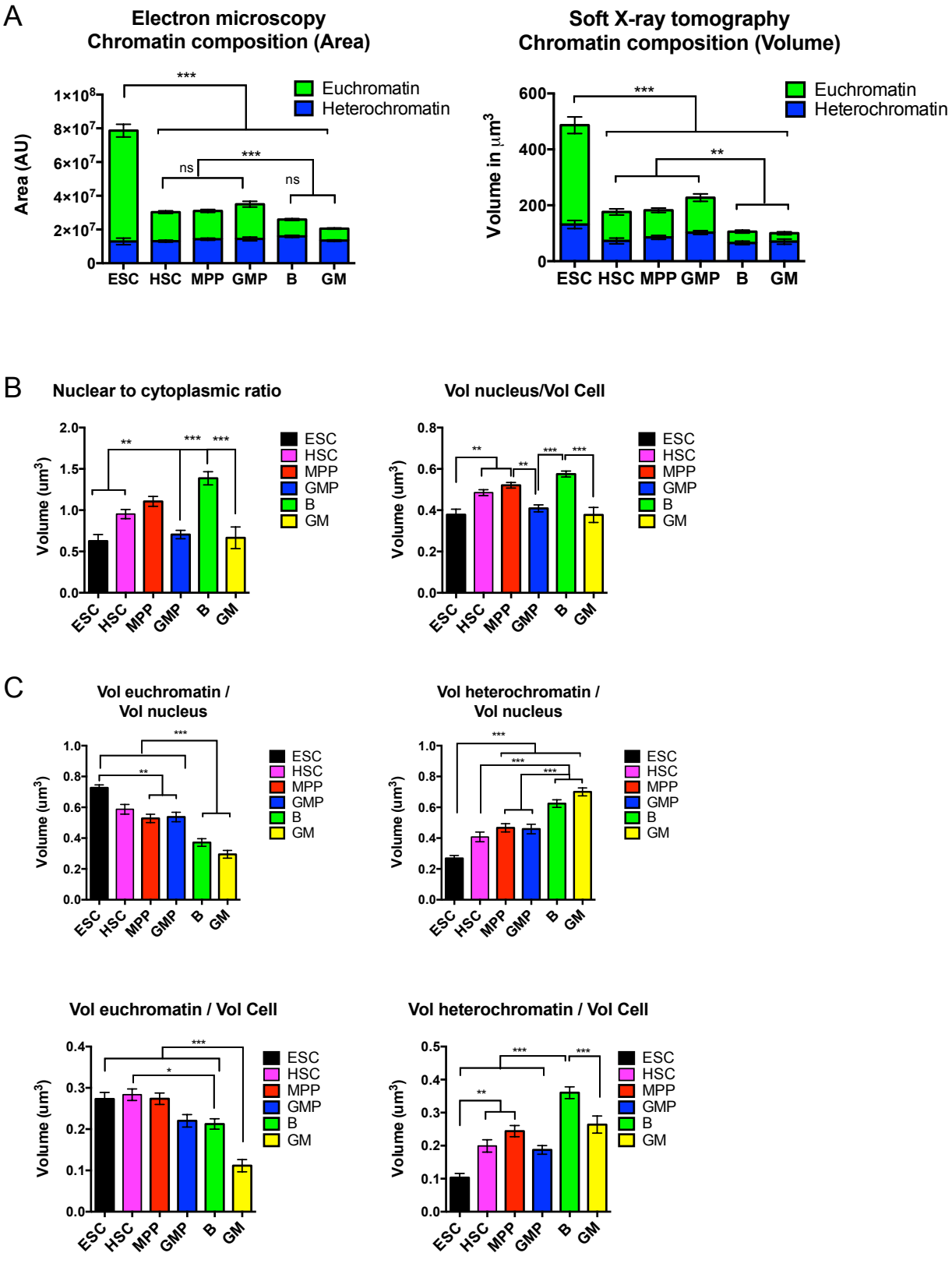

Supplemental Figure 2. Progressive changes in euchromatin content and nuclear size during stem cell differentiation; related to Figure 2

(A) Quantification of the area (by EM) and volume (by SXT) of hetero- and eu-chromatin in ESCs, HSCs, MPPs, GMPs, B and GM cells. Both analyses demonstrated that the amount of euchromatin is reduced dramatically upon stem cell differentiation, whereas the amount of heterochromatin remains relatively stable. Statistical significant differences refer to amount of euchromatin. n = 30 per cell type for EM; n = 8 per cell type for SXT in 3 or more experiments.

(B) The nuclear to cytoplasmic ratio (left panel) and the ratio of nuclear size to the total cell size (right panel) are significantly higher in B cells, HSCs and MPPs than in ESCs, GMPs and GM cells. Measures were made using SXT. (n = 8 per cell type in 3 or more experiments).

(C) Comparison between nuclear or cell size and the total volumes of heterochromatin or euchromatin revealed that the nuclear and cell volumes gradually change with compaction of euchromatin into heterochromatin. Measures were made using SXT. (n = 8 per cell type in 3 or more experiments).

Data are means ± SEM, *$p < 0.05$, **$p < 0.01$, ***$p < 0.001$, ns not significant. Statistics by one-way anova.

Supplemental Figure 3

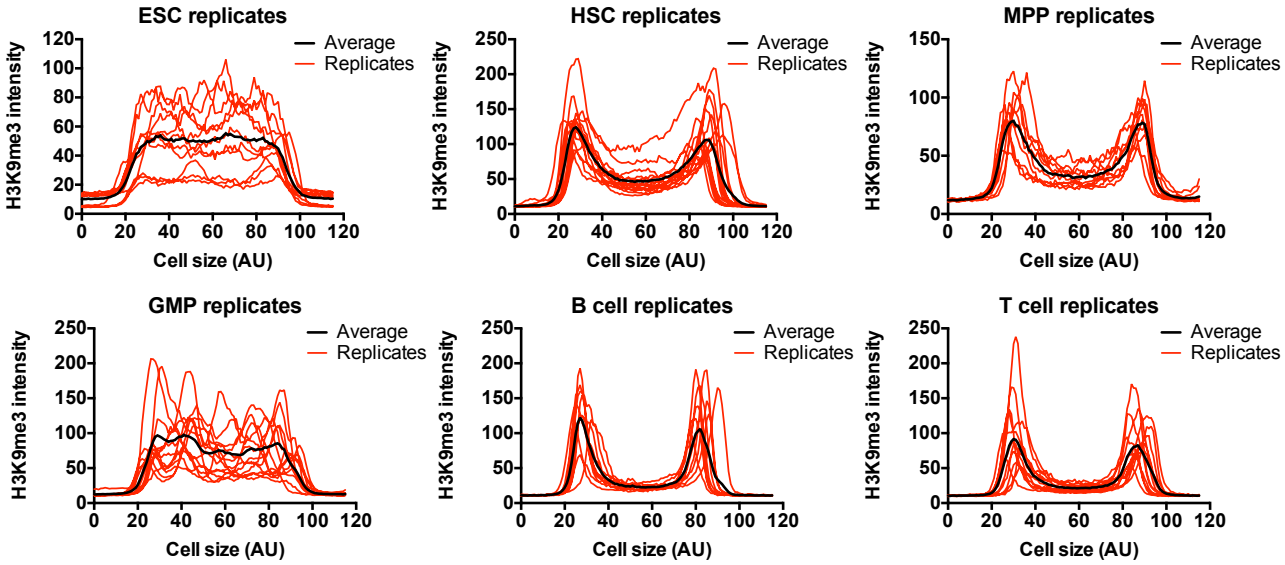

Supplemental Figure 3. The subnuclear distribution of the heterochromatin mark H3K9me3 changes upon stem cell differentiation; related to Figure 3

The radial distribution of H3K9me3 was quantified by fluorescence intensity across the middle section of individual ESCs, HSCs, MPPs, GMPs, B and T cells. Each red line represents the fluorescence intensity across a single cell. Although the averaged values for multiple individual cells (shown here as a black line, and as a red line in Figure 3B) do not distinguish between ESCs and GMPs, individual replicate analyses show that ESCs have a more homogenous distribution of H3K9me3 across their nuclei, whereas GMPs have distinct foci of high intensity randomly distributed within their nuclei. In contrast, HSCs, MPPs, B and T cells display H3K9me3 distribution in increasingly close proximity to the nuclear envelope.

Supplemental Figure 4

A

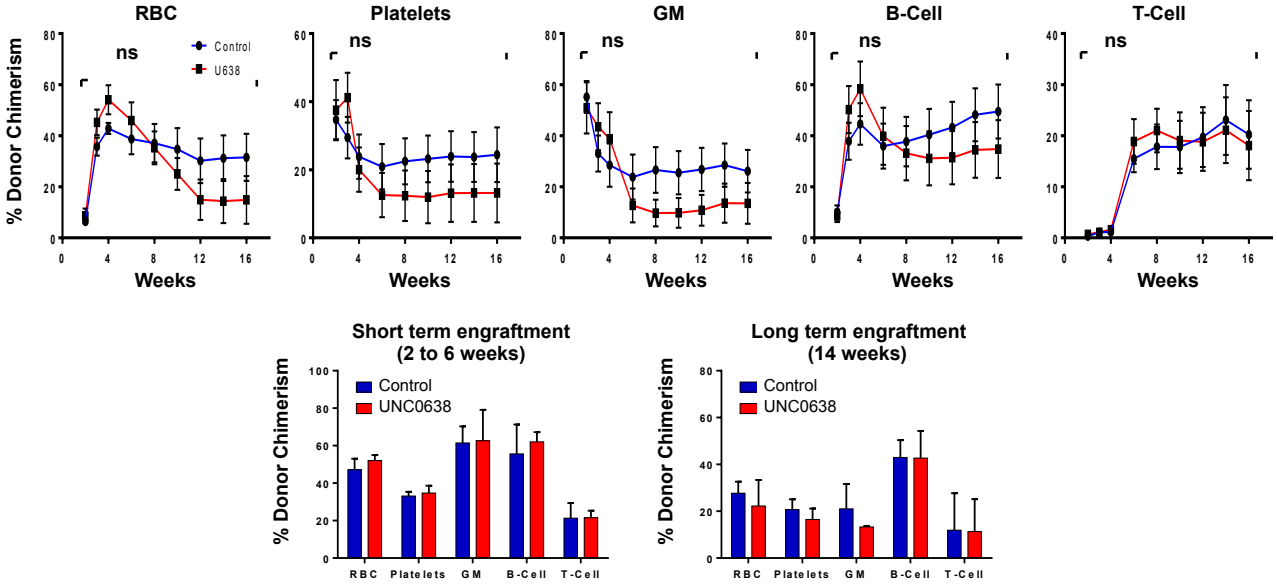

B

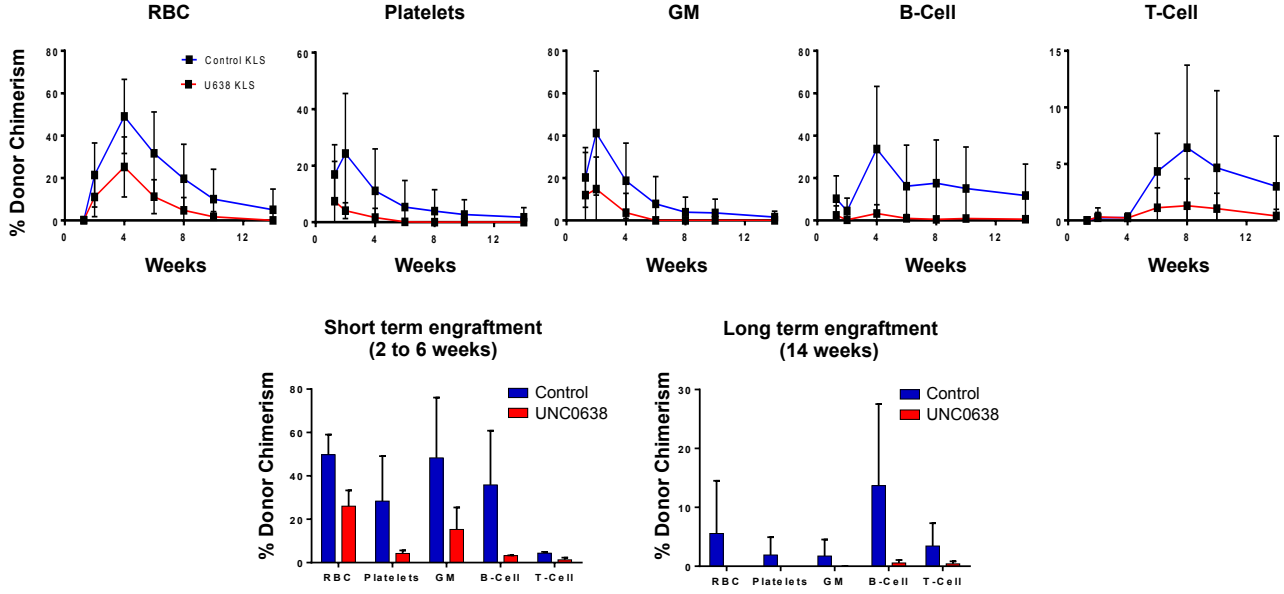

Supplemental Figure 4. Inhibition of G9A in HSCs *in vitro* does not improve hematopoietic reconstitution; related to Figure 5

(A) HSCs cultured for 5 days on AFT024 cells with UNC0638 showed no significant differences in hematopoietic reconstitution compared to the untreated (DMSO) control cells. HSCs (KLS $FLK2^-$ $CD150^+$ BM cells) were isolated from UBC-GFP mice and grown on AFT024 cells for 5 days with or without the G9A inhibitor UNC0638. Equal numbers of cells harvested from control or UNC0638 wells were injected into irradiated recipient mice. Reconstitution was measured by quantification of donor contribution to mature cells in the peripheral blood. Line graphs display the peripheral blood reconstitution of each lineage over time for one out of three independent experiments, each performed with at least 3 recipient mice. Bar graphs display the short-term (left graph; measured at 2-6 weeks post-transplantation depending on cell type) or long-term (right graph; measured >14 weeks post-transplantation for all cell types) reconstitution for each lineage for all three experiments. n = 3 independent experiments with 3-5 recipient mice per group. P-values were determined using 2-way ANOVA. No significant differences were observed.

(B) HSCs cultured for 5 days with UNC0638 showed no significant differences in hematopoietic reconstitution compared to the untreated (DMSO) control cells. The experiment was performed as in (A), expect cells were grown in liquid culture without AFT024 cells. n = 2 independent experiments with 7-10 recipient mice per group. P-values were determined using 2-way ANOVA. No significant differences were observed.

Supplemental Figure 5

A

GO category	GO pathway	p-value
KEGG Pathway	leukocyte transendothelial migration	1.44E-03
	ecm receptor interaction	1.70E-03
	cell adhesion molecules	6.96E-03
GO Biological Processes	hemostasis (GO:0007599)	1.57E-12
	blood coagulation (GO:0007596)	3.36E-12
	coagulation (GO:0050817)	3.36E-12
	leukocyte migration (GO:0050900)	7.91E-10
	regulation of response to wounding (GO:1903034)	6.98E-09
	integrin-mediated signaling pathway (GO:0007229)	1.92E-08
	regulation of cell activation (GO:0050865)	2.68E-08
	leukocyte activation (GO:0045321)	3.22E-07
	platelet activation (GO:0030168)	1.15E-06
	regulation of platelet activation (GO:0010543)	1.41E-06
GO Cellular Component	integral component of plasma membrane (GO:0005887)	1.05E-08
	side of membrane (GO:0098552)	7.68E-08
	external side of plasma membrane (GO:0009897)	9.17E-08
	extracellular vesicular exosome (GO:0070062)	2.68E-07
	cell surface (GO:0009986)	1.16E-06
	anchoring junction (GO:0070161)	3.17E-06
	adherens junction (GO:0005912)	1.03E-05
Molecular Function	cell adhesion molecule binding (GO:0050839)	4.75E-05
	cytokine receptor activity (GO:0004896)	8.55E-05
	actin binding (GO:0003779)	1.32E-04
	guanyl-nucleotide exchange factor activity (GO:0005085)	7.57E-04
	purinergic nucleotide receptor activity (GO:0001614)	9.94E-04
	nucleotide receptor activity (GO:0016502)	9.94E-04
	immunoglobulin binding (GO:0019865)	1.74E-03
	heparin binding (GO:0008201)	1.76E-03
	Ras guanyl-nucleotide exchange factor activity (GO:0005088)	2.03E-03

B

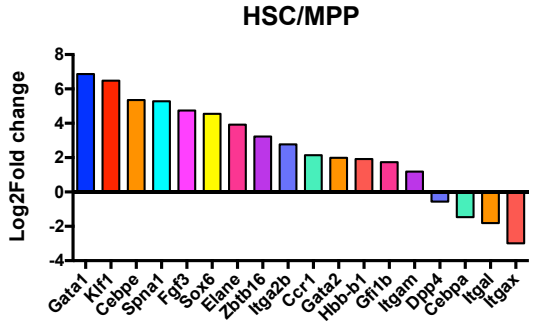

C

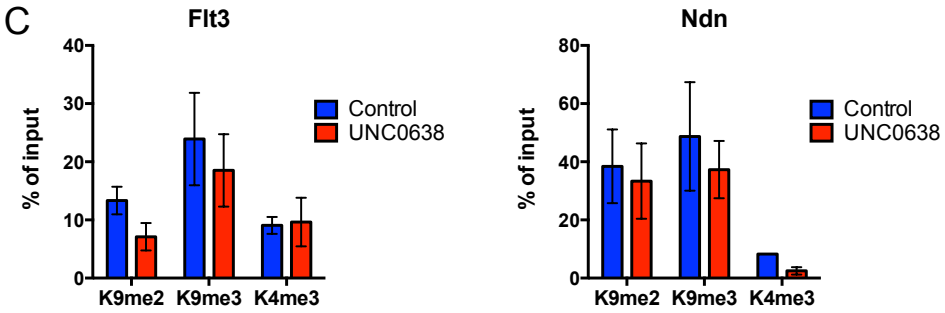

Supplemental Figure 5. Effect of G9A inhibition on HSC differentiation *in vitro*; related to Figure 5

(A) Gene Ontology (GO) term analysis of genes differentially regulated between control and UNC0638-treated HSCs. Experimental conditions for HSC culturing and RNAseq were described in Figure 5. GO analysis was performed using the EnrichR tool (http://amp.pharm.mssm.edu/Enrichr/; Chen et al., 2013) on 650 differentially regulated genes.

(B) Differential gene expression (log2fold change) between freshly isolated HSCs and MPPs of a subset of genes identified to be similarly regulated by G9A upon *in vitro* HSC culture in the absence and presence of UNC0638.

(C) ChIP-qPCR analysis showed that genes down-regulated genes upon UNC0638 treatment do not display significant reductions in the levels of H3K9me2 at their promoter, in contrast to genes which were upregulated upon UNC0638 treatment (Figure 4E). Data are displayed as means ± SEM; n=3 with each qPCR reaction run in triplicate from 3 independent experiments. No significant differences were observed.

MOVIE LEGEND

Movies S1-S3: Nuclear architecture is distinctly different during stem cell differentiation into mature cells; related to Figure 2.

Soft X-ray Tomography was used to image whole, fully hydrated cells. The movies feature the cell (grey) and the shape of the nucleus (blue), euchromatin (green), nucleoli (red), lipid bodies (yellow) and mitochondria (gold) of an embryonic stem cell (ESC; Movie S1), a granulocyte/monocyte progenitor cell (GMP; Movie S2) and a mature granulocyte/monocyte (Movie S3) by imaging through the entire cell.

SUPPLEMENTAL EXPERIMENTAL PROCEDURES

Cell isolation

Hematopoietic cell populations were isolated from the BM of murine femurs and tibias. Stem and progenitor cell fractions were enriched using CD117-coupled magnetic beads (Miltenyi). Cells were stained with unconjugated lineage rat antibodies (CD3, CD4, CD5, CD8, B220, GR1, MAC1, and TER119; Biolegend, Cat #s 100331, 100402, 100602, 100702, 103202, 108402, 101202, and 116202) followed by goat-α-rat PE-Cy5 (Biolegend, Cat # A10691). Stem cells were isolated using c-KIT-APC-Cy7, SCA1-PB, SLAMF1-PECy7, CD34-FITC, FcγrII-PE and FLK2-biotin (Biolegend, Cat #s 105814, 122520, 115914, 101308, 135308; anti-CD34-FITC was from eBioscience, Cat # 11-0341-85) followed by streptavidin-Qdot605 (Invitrogen, Cat # Q10101MP). Cells were sorted using a FACS Aria II (BD Bioscience). HSPCs were defined as c-KIT$^+$Lin$^-$SCA1$^+$ (KLS) BM cells; HSCs as either FLK2$^-$ and/or CD150$^+$ KLS cells, as indicated; MPPs as FLK2$^+$ KLS cells; myeloid progenitors as c-KIT$^+$Lin$^-$SCA1$^-$ BM cells and mature hematopoietic cells as positive for cell surface expression of CD3 (T cells), CD4, CD5, CD8, B220 (B cells), GR1, MAC1 ("GM" cells were positive for both GR1 and MAC1), and/or TER119 (Beaudin et al., 2014; Boyer et al., 2011; Forsberg et al., 2006; Smith-Berdan et al., 2015). Embryonic stem cells (ESC) E14 were cultured as previously described (Gaspar-Maia et al., 2009).

Nuclease sensitivity

FACS sorted cells were washed once with cold PBS 1% BSA and then resuspended in chromatin buffer (10 mM Tris pH 7.8, 85 mM KCl, 0.5 mM spermidine, 0.15 mM spermine, 5% sucrose, 1% BSA, 0.1 % Saponin, 3mM MgCl2). Cell aliquots were incubated for 6 min at 37°C with increasing concentrations (ranging from 0.2-2 units) of DNaseI (Worthington) diluted in chromatin buffer. Micrococcal nuclease digestion (0.1-1 units) was performed using chromatin buffer plus 1mM CaCl2. Nuclease reactions were stopped by adding equal volume of lysis buffer (10mM Tris pH 7.8, 0.1M EDTA, 10mM EGTA, 0.5% SDS), 0.4 mg/ml proteinase K and 20 ug/mL of RNase and incubated at 42°C for 2 hours. DNA was isolated using phenol/chloroform, and analyzed on 1% agarose gel with

SyberGold (Invitrogen). $1x10^4$ sorted cells were used per datapoint. For the mobilization experiment of Figure S1A, mice were mobilized with cytoxan and G-CSF (Cy/G) as previously described (Morrison et al., 1997; Smith-Berdan et al., 2011).

DNA methylation

For DNA methylation assays we used the restriction enzymes MspI and HpaII, which recognize the identical DNA sequence (CCGG), but have different methylation sensitivity: HpaII activity is blocked by the presence of CpG methylation. Isolated gDNA (0.5ug) was digested overnight at 37°C with various combinations of MspI, HpaII, and HindIII; and analyzed on 1% agarose gel with SyberGold. HindIII was used as a general nuclease to increase the fragmentation size of gDNA. The methylation status of the DNA was established by measuring, for each lane, the ratio between the signal present between 1.5 kb and 5 kb, and the totality of the smear. Relative methylation was calculated as the ratio between the values obtained for MspI and HpaII digestion for each DNA sample.

Histone western blot and immunohistochemistry

For western blots, $1x10^4$ FACS sorted cells were lysed in RIPA buffer, and run in a 15% gradient SDS-page (BIO-RAD). Histone modifications were assessed with antibodies against H3K27me3 (07-449 Millipore), H3 Acetylated (06-599), H4K16Ac (07-329), H3K4me3 (07-473), total H3 (06-755), H3K36me3 (Ab9050, Abcam), H3K9me2 (Ab1220), H3K9me3 (Ab8898), and H4K20me1 Ab9051). Cells were incubated with the HDAC inhibitor trichostatin A (Cell signaling) at 37°C for 2 hours to induce histone acetylation. With the exception of increased H3Ac in TSA treated samples, P-values were greater than 0.05 for all comparisons. ESCs *vs* HSPCs: H3K4me3, > 0.9999; H3Ac, > 0.9999; H4K16Ac, 0.122; H3K36me3, 0.2227; H3K27me3, > 0.9999; H3K9me2, 0.7049; H3K9me3, > 0.9999. ESCs *vs* mature cells: H3K4me3, > 0.9999; H3Ac, > 0.9999; H4K16Ac, > 0.9999; H3K36me3, 0.409; H4K20me1, 0.3430; H3K27me3, > 0.9999; H3K9me2, > 0.9999; H3K9me3, > 0.9999. HSPCs *vs* mature cells: H3K4me3, > 0.9999; H3Ac, > 0.9999; H4K16Ac, 0.0568; H3K36me3, > 0.9999; H3K27me3, > 0.9999; H3K9me2, > 0.9999; H3K9me3, > 0.9999.

For immunostaining, cells were sorted and placed into poly-lysine coated slides, fixed with 2% PFA, permeabilized with 0.1% triton-x in PBS, and stained with H3K9me3 (Abcam, Ab8898), Lamin B (Santa Cruz Biotechnology, sc-6217) antibodies followed by an Alexa488-Donkey-α-goat and a Alexa594-goat-α-rabbit secondary antibody (Invitrogen, Cat #s A11055 and A11037) plus DAPI. Images were acquired using a PerkinElmer Volocity spinning disk confocal microscope. Image analysis was done using ImageJ software (Schneider et al., 2012).

Nucleosome ELISAs

ELISAs to measure the abundance of histones and histone modifications of different cell populations were performed by adaptation of a previously published nucleosome (NU-)ELISA protocol (Dai et al., 2013). Briefly, mononucleosomes from about $1x10^6$ cells were acid extracted, quantified by Quant-iT Pico Green assay (Life Technologies, Carlsbad, CA), and loaded onto plates in serial dilutions. Anti-H2A (NB100-56346, Novus Biologicals), H3Ac, H4K16Ac, H3K36me3, H4K20me1, H3K27me3, H3K9me2, H3K9me3 and the appropriate anti-rabbit (406401, Biolegend) or anti-mouse (405306, Biolegend) HRP-conjugated secondary antibodies were used; we were unable to obtain reliable dose-response curves using anti-H3 and anti-H3K4me3 antibodies. Plates were developed using Ultra-TMB (Thermo Fisher), terminated using 1.5 M sulfuric acid, and the absorbance read at 450nm using a SpectraMax plate reader (Molecular Devices). Data were normalized the H2A signal from each cell type from the linear region of dose-response curves (typically 150-600 pg chromatin; Figure S1D). With the exception of increased H3Ac in TSA treated samples, P-values were found to be greater than 0.05 for all comparisons: H3Ac, 0.3314; H4K16Ac, 0.3453; H3K36me3, 0.1316; H4K20me1, 0.9597; H3K27me3, 0.0709; H3K9me2, 0.3262; H3K9me3, 0.2004.

Electron microscopy

For electron microscopy, cells were fixed in 2% glutaraldehyde, 1% paraformaldehyde in 0.1M sodium cacodylate buffer pH 7.4, post fixed in 2% osmium tetroxide in the same buffer, in block stained with 2% aqueous uranyl acetate, dehydrated in acetone, infiltrated, and embedded in LX-112 resin (Ladd

Research Industries, Burlington, VT). Samples were ultrathin sectioned on a Reichert Ultracut S ultramicrotome and counter stained with 0.8% lead citrate. Grids were examined on a JEOL JEM-1230 transmission electron microscope (JEOL USA, Inc., Peabody, MA) and photographed with the Gatan Ultrascan 1000 digital camera (Gatan Inc., Warrendale, PA) at the electron microscopy facility of the Gladstone Institute (San Francisco, CA). Electron-dense nuclear areas were defined as heterochromatin as illustrated in Figure 2B. Image analysis was done using ImageJ software (Schneider et al., 2012).

Soft X-ray microscopy

FACS sorted cells were mounted in thin-walled glass capillary tubes and rapidly cryo-immobilized prior to being mounted in the cryogenic specimen rotation stage of the XM-2 Soft X-ray microscope, at the National Center for X-ray Tomography located at the Advanced Light Source of Lawrence Berkeley National Laboratory. Each dataset (i.e. 90 projection images spanning a range of 180◦) was collected using a Fresnel zone plate-based objective lens with a resolution of 50 nm (Le Gros et al., 2005). The projections for every tilt were recorded using a Peltier cooled, back-thinned and direct illuminated 2048*2048 pixel soft x-ray CCD camera (Roper Scientific iKon-L, Trenton, NJ, USA). Projection images were manually aligned using IMOD software by tracking fiducial markers on adjacent images (Kremer et al., 1996). The 3D X-ray tomograms were hand-segmented using Amira software (Visualisation Science Groups, FEI company), and used to reconstruct volumes, measure voxel values (i.e. absorption values in volume element of the reconstructed data), to calculate linear absorption coefficients (LACs) and create supplementary movies. Each subcellular component attenuates soft X-rays differently and quantitatively, such that distinct organelles, including eu- and heterochromatin, can be identified and quantified in 3D (Le Gros et al., 2005; McDermott et al., 2009; Parkinson et al., 2013).

HSC in vitro culture and transplantation

FACS sorted HSCs (KLS FLK2-SLAMF1+) were seeded at 100-500 cells into 96-well plates and cultured with X-vivo15 (Lonza) supplemented with 25ng/ml SCF, 5ng/ml TPO, primocin and B-ME. Alternatively, HSCs were incubated on ATF024 feeder layers cells (a gift from Dr. Kateri Moore; also available from ATCC, SCRC-1007), and maintained in DMEM, 10%FCS, Pen/strep, with 25ng/ml SCF, 5ng/ml TPO. AFT024 layers were setup to 80% confluence the day before the co-culture with HSCs. G9A inhibitor UNC0638 (Sigma) and control DMSO were used at 0.3uM final concentrations. After 24 hours in X-vivo culture, cells were transplanted into lethally irradiated C57BL/6 mice together with $2x10^5$ Sca-1 depleted BM cells. After 5 days in culture on AFT024 layers, cells were trypsinized and analyzed for stem cell surface marker expression by FACS (Lineage neg, Kit+, Sca-1+). Hematopoietic cells were separated from the AFT024 cells based on the GFP expression of hematopoietic cells as HSCs were derived from UBC-GFP mice). Equal numbers of Kit+ or KLS cells were then transplanted into lethally irradiated C57BL/6 mice together with $2x10^5$ Sca-1 depleted BM cells. For Figures 5 and S4B, HSCs were grown in liquid culture for 24 hrs (Figure 5) or 5 days (Figure S4B) before transplantation; for Figure S4A HSCs were grown on AFT024 cells for 5 days. Short-term reconstitution was defined as the timepoint post-transplantation after which reconstitution levels plateaued or started to decline; this ranged from 2 (Plt and GM) to 6 (T cells) weeks post-transplantation. Long-term reconstitution was defined as >14 weeks post-transplantation. Consistent with previous reports (Moore et al., 1997; Nolta et al., 2002), use of AFT024 cells enhanced the ability of cultured HSCs to engraft long-term. *In vitro* migration assays were performed in 5 mm pore size transwell inserts (Corning) towards SDF1 (100 ng/ml, Peprotech) for 2 hours at 37°C, as described previously (Smith-Berdan et al., 2011). Cell cycle analyses were performed using the Click iT EdU assay (Life Technologies) as per manufacturer's instructions.

Gene expression and ChIP-qPCR

RNA-seq libraries from *in vitro* cultured cells were prepared using NEBNext® Ultra kit (New England Biolabs) following manufacturer instructions. Libraries were sequenced using HiSeq2000 platform

(Illumina) at the genomic sequencing laboratory, UC Berkeley, and analyzed with DESEQ software (Bioconductor.org). The intersect of differentially regulated genes was assessed by php coding and the p-value calculated by hypergeometric test (http://nemates.org/MA/progs/overlap_stats.html). GO analysis was performed using the EnrichR tool (http://amp.pharm.mssm.edu/Enrichr/; Chen et al., 2013) on the 650 genes differentially regulated between control and UNC0638-treated HSCs. ChIP experiments were performed on *in vitro* cultured, FACS sorted, hematopoietic cells using SX-8G IPSTAR automated ChIP system (Diagenode) using 1ug of H3K4me3 (Millipore, 07-473), H3K9me2 (Abcam, Ab1220), and H3K9me3 (Abcam, Ab8898) antibodies respectively. qPCR on ChIP DNA were performed with SensiMix SYBR® No-ROX kit (Bioline) and the ViiA7 system (Life Technologies).

SUPPLEMENTAL REFERENCES

Beaudin, A.E., Boyer, S.W., and Forsberg, E.C. (2014). FLK2/Flt3 promotes both myeloid and lymphoid development by expanding non-self-renewing multipotent hematopoietic progenitor cells. Exp Hematol *42*, 218-229 e214.

Boyer, S.W., Schroeder, A.V., Smith-Berdan, S., and Forsberg, E.C. (2011). All Hematopoietic Cells Develop from Hematopoietic Stem Cells through FLK2/Flt3-Positive Progenitor Cells. Cell Stem Cell *9*, 64–73.

Chen, E.Y., Tan, C.M., Kou, Y., Duan, Q., Wang, Z., Meirelles, G.V., Clark, N.R., and Ma'ayan, A. (2013). Enrichr: interactive and collaborative HTML5 gene list enrichment analysis tool. BMC Bioinformatics *14*, 128.

Dai, B., Giardina, C., and Rasmussen, T.P. (2013). Quantitation of nucleosome acetylation and other histone posttranslational modifications using microscale NU-ELISA. Methods Mol Biol 981, 167-176.

Forsberg, E.C., Serwold, T., Kogan, S., Weissman, I.L., and Passegué, E. (2006). New evidence supporting megakaryocyte-erythrocyte potential of FLK2/flt3+ multipotent hematopoietic progenitors. Cell *126*, 415–426.

Gaspar-Maia, A., Alajem, A., Polesso, F., Sridharan, R., Mason, M.J., Heidersbach, A., Ramalho-Santos, J., Mcmanus, M.T., Plath, K., Meshorer, E., et al. (2009). Chd1 regulates open chromatin and pluripotency of embryonic stem cells. Nature *460*, 863–868.

Le Gros, M.A., McDermott, G., and Larabell, C.A. (2005). X-ray tomography of whole cells. Curr. Opin. Struct. Biol. *15*, 593–600.

McDermott, G., Le Gros, M.A., Knoechel, C.G., Uchida, M., and Larabell, C.A. (2009). Soft X-ray tomography and cryogenic light microscopy: the cool combination in cellular imaging. Trends Cell Biol *19*, 587–595.

Moore, K.A., Ema, H., and Lemischka, I.R. (1997). In vitro maintenance of highly purified, transplantable hematopoietic stem cells. Blood *89*, 4337–4347.

Morrison, S.J., Wright, D.E., and Weissman, I.L. (1997). Cyclophosphamide/granulocyte colony-stimulating factor induces hematopoietic stem cells to proliferate prior to mobilization. Proc Natl Acad Sci USA *94*, 1908–1913.

Nolta, J.A., Thiemann, F.T., Arakawa-Hoyt, J., Dao, M.A., Barsky, L.W., Moore, K.A., Lemischka, I.R., and Crooks, G.M. (2002). The AFT024 stromal cell line supports long-term ex vivo maintenance of engrafting multipotent human hematopoietic progenitors. Leukemia *16*, 352–361.

Parkinson, D.Y., Epperly, L.R., McDermott, G., Le Gros, M.A., Boudreau, R.M., and Larabell, C.A. (2013). Nanoimaging cells using soft X-ray tomography. Methods Mol Biol *950*, 457–481.

Schneider, C.A., Rasband, W.S., and Eliceiri, K.W. (2012). image J. Nat Meth *9*, 671–675.

Smith-Berdan, S., Nguyen, A., Hassanein, D., Zimmer, M., Ugarte, F., Ciriza, J., Li, D.Y., García-Ojeda, M.E., Hinck, L., and Forsberg, E.C. (2011). Robo4 cooperates with CXCR4 to specify hematopoietic stem cell localization to bone marrow niches. Cell Stem Cell *8*, 72–83.

Smith-Berdan, S., Nguyen, A., Hong, M.A., and Forsberg, E.C. (2015). ROBO4-mediated vascular integrity regulates the directionality of hematopoietic stem cell trafficking. Stem Cell Reports *4*, 255-268.